NANOSYSTEMS:
PHYSICS, CHEMISTRY, MATHEMATICS

Lwin H.M., Yarovaya O.V. *Nanosystems: Phys. Chem. Math.*, 2024, **15** (4), 487–497.
http://nanojournal.ifmo.ru
DOI 10.17586/2220-8054-2024-15-4-487-497

Original article

Colloidal chemical properties of the sol $V_2O_5 \cdot nH_2O$

Hein Myat Lwin[a], Oksana V. Yarovaya[b]

D. I. Mendeleev University of Chemical Technology of Russia, Moscow, Russia

[a]heinmyatlwin2468@gmail.com, [b]iarovaia.o.v@muctr.ru

Corresponding author: Oksana V. Yarovaya, iarovaia.o.v@muctr.ru

PACS 82.70.Dd

ABSTRACT The colloidal properties of the lyophilic dispersion system $V_2O_5 \cdot nH_2O$ sol studied in this work was obtained by the thermolysis of V_2O_5 powder with hydrogen peroxide. The dispersion phase exists in the form of nanorods. The optimal mole ratio of V_2O_5 and H_2O_2 for synthesizing the sol is 1:30, and the possible concentration of V_2O_5 in the entire colloidal system ranges between 0.3 to 1.6 mass percent. The existence of nanoparticles in this colloidal system and the pH range that maintains the stability of the sol conform to the phase diagram of vanadium (V) in an aqueous medium. The absolute value of the zeta potential of the sol increases when the initial concentration of the sol during synthesis increases and the ionic strength of the dispersion medium decreases. Potential curves of pair interaction between nanoparticles were also constructed according to the DLVO theory.

KEYWORDS $V_2O_5 \cdot nH_2O$, thermolysis, nanorods, lyophilic colloidal system, stability, DLVO theory

FOR CITATION Lwin H.M., Yarovaya O.V. Colloidal chemical properties of the sol $V_2O_5 \cdot nH_2O$. *Nanosystems: Phys. Chem. Math.*, 2024, **15** (4), 487–497.

1. Introduction

In recent years, one can see rapid progress in the field of nanotechnology with a particular focus on the synthesis and applications of nano-scale materials. Among these, vanadium (V) oxide (V_2O_5) sol has attracted significant attention due to its unique properties and potential applications in such fields as catalysis, energy storage, sensors, and optics [1–3]. V_2O_5 is a widely studied transition-metal oxide with a layered crystal structure, featuring strong Vanadium-Oxygen bonds [4, 5]. In the field of catalysis, V_2O_5 has demonstrated exceptional performance as a catalyst for oxidation, hydrogenation, and dehydrogenation reactions due to its high surface area and redox properties [6–11]. Moreover, V_2O_5 shows promise for use in energy storage devices, such as lithium-ion batteries and supercapacitors, owing to its electronic conductivity and electrochemical stability [12, 13]. Additionally, the potential use of V_2O_5 in gas sensing, electrochromic devices, and optical coatings further highlights its significance in emerging technologies [14–16].

V_2O_5 sol, comprising nanoscale V_2O_5 particles suspended in a liquid medium, offers significant advantages such as high surface area, tunable properties, and enhanced reactivity, thereby opening up new perspectives for its practical utilization. The preparation of V_2O_5 sol involves the synthesis of nanoscale V_2O_5 particles, followed by their dispersion in a suitable liquid medium. Over the years, various methods have been developed to prepare V_2O_5 sol, each offering distinct advantages and disadvantages. The choice of synthesis method is critical in determining the particle size, morphology, and surface properties of the resulting V_2O_5 sol, which in turn dictate its performance in different applications [17–26].

The sol-gel method has been used to create V_2O_5 thin films and nanopowders from V_2O_5 sols, which were prepared by ion exchange [17, 18], alkoxide hydrolysis [19, 20], solidification melting [21–23] and hydrolysis/thermolysis of V_2O_5 using hydrogen peroxide [24–26]. Among these methods, the method of hydrolysis/thermolysis of V_2O_5 using hydrogen peroxide is attractive due to its environmental safety, low cost, and simplicity of the process [27]. There are many articles [24–30] on the process and application of the $V_2O_5 \cdot nH_2O$ sol/gel obtained by this method. However, the assessment of the colloidal stability of the sol obtained by these methods was not reported in the available literatures.

The colloidal chemical properties of V_2O_5 sols play a crucial role in determining their performance in diverse applications. Studying the colloidal stability of V_2O_5 sols can provide valuable insights into the underlying physicochemical mechanisms, such as particle-particle interactions, surface properties, and the influence of various factors (pH, ionic strength, concentration, etc.). This fundamental understanding is essential for the rational design and optimization of V_2O_5-based materials and systems.

By gaining a deeper understanding of the colloidal properties of V_2O_5 sols, researchers can optimize their performance and develop new applications with enhanced reactivity, stability, and sensitivity. For instance, improved colloidal stability can lead to enhanced dispersibility, processability, and long-term performance of V_2O_5-based materials in various fields, including catalysis, energy storage, and functional coatings. Therefore, the synthesis of V_2O_5 and a comprehensive

investigation of its colloidal properties become important areas of study. This study can provide valuable insights for the development of advanced V_2O_5-based materials and technologies.

2. Materials and methods

2.1. Materials

The following reagents were used in the work: vanadium (V) oxide, "analytical grade"; and hydrogen peroxide H_2O_2, "special purity grade" are used as the sources of sol preparation.

2.2. Method for preparation of sol

Distilled water was added to the round bottom flask containing V_2O_5 powder and dispersed by stirring. Then the calculated volume of hydrogen peroxide solution was added and stirred until a homogeneous yellow mass was formed. Then the required amount of water was added and heated to a boil using a reverse refrigerator. After boiling for 5 minutes, the color changes from yellow to orange, and then after 3 minutes, it turns into dark red resulting $V_2O_5 \cdot nH_2O$ sol.

2.3. Method for determining the concentration of vanadium (V) in solutions and sols

To determine vanadium (V), titrated using Mohr's salt $(NH_4)_2Fe(SO_4)_2$. Previously, 5 M sulfuric acid was added to the analyzed solution in a volume ratio of 1:1. Phenylanthranilic acid was used as an indicator, based on the acidity of the medium. The equivalence point was determined when the solution transitioned from violet to green. The permissible absolute total error of the analysis is 0.7 %, with a confidence level of $P = 0.95$ [31].

The reaction occurred during titration is described in eq. (1).

$$2H_3VO_4 + 2(NH_4)2Fe(SO_4)_2 + 2H_2SO_4 \rightarrow V_2O_2(SO_4)_2 + Fe(SO_4)_3 + 2(NH_4)_2SO_4 + 6H_2O. \quad (1)$$

The concentration of vanadium (V) content was calculated using formulas (2) and (3).

$$\text{Vanadium(V) concentration, mole/liter} = \frac{V_{\text{avg}} \times N}{V_{\text{analyz}} \times 2}, \quad (2)$$

$$V_2O_5,\ \text{g/l} = \frac{V_{\text{avg}} \times N \times 91}{V_{\text{analyz}}}, \quad (3)$$

where: N is the normality of Mohr's salt solution $(NH_4)_2Fe(SO_4)_2$, mole/liter; V_{avg} is the average volumes of Mohr's salt used for titration, ml; V_{analyz} is the volume of the analyzed solution (10 ml); 91 is the equivalent mass of vanadium oxide.

2.4. Characterization

The morphology and particle size of nanoparticles were analyzed by the Transmission Electron Microscope (TEM) LIBRA 200 FE HR (Germany). Absorption spectra of sol were recorded on a brand spectrophotometer LEKI SS2110UV in plastic cuvettes with an absorbing layer thickness of 10 mm in the wavelength range 500 – 800 nm. pH determination was carried out on a pH-meter/milivoltmeter (pH-420) OOO device using a glass electrode, the measurement range of which is from 0.5 to 14. The determination of zeta potential was carried out on a Compact-Z device using standard round cuvettes measuring 15×45 mm with a capacity of 4 ml, with a relative measurement error of ± 1 %.

The content of particles in the resulting sol was determined by acidimetric titration according to the method in Section 2.3. First, we analyzed the total vanadium (V) content and the vanadium (V) content in the filtrate, which was obtained after ultrafiltration using an ultrafiltration cell with a UPM-450 polymer membrane. Based on these experimental results of total concentration and the concentration of filtrate, the content of vanadium (V) particles was determined. The ionic strength of the dispersion medium was calculated based on the obtained data on the concentration of dissolved V_2O_5 in the resulting filtrate.

The threshold for rapid coagulation is determined by the threshold volume of the electrolyte at which the optical density of the sol reaches its maximum value, and does not change with further addition of electrolyte. Coagulation threshold values C_{crit} were calculated using eq. (4).

$$C_{\text{crit}} = \frac{C_{\text{elect}} \times V_{\text{crit}}}{V}, \quad (4)$$

where: C_{elect} is the concentration of electrolyte (mol/l), V is the volume of the system (ml).

The morphology of the thin layer was analyzed by Scanning Electron Microscope (SEM) JEOL 1610LV(JEOL, Japan). The crystallographic structure of the sample was analyzed using powder X-ray diffraction DX-2700BH (XRD, with CuKα radiation).

2.5. Calculation method for potential energy of paired particle interactions using DLVO theory

At first, the value of the complex Hamaker constant was calculated. According to the DLVO theory, for the electrolyte concentration equals to the rapid coagulation threshold, the potential curve of the dispersed system is in the region of negative values. Only its maximum, corresponding to the zero potential barrier, lies on the abscissa axis. So, the value of the complex Hamaker constant for the hydrosols was determined graphically, taking the ionic strength of the dispersion medium equal to the sum of the ionic strength of a freshly prepared sol and the value of the rapid coagulation threshold in the presence of an indifferent electrolyte of type 1–1 ($NaNO_3$).

Assuming that the particles are in the form of cylinders, the molecular component of the potential energy of pair interaction for two particles through a layer of dispersion medium was calculated using equation (5) [32]:

$$U_{\text{m,cylinder}} = -\frac{A_{131}l}{12\sqrt{2}h^{3/2}}\left[\frac{a_1a_2}{a_1+a_2}\right]^{1/2}, \tag{5}$$

where: A_{131} is the complex Hamaker constant, characterizing the interaction of two particles of a certain nature through a layer between them, Joule (1 indicates the nature of the interacting particles, 3 – the layer); h is the distance between particles, m; a_1 and a_2 are the radii of the interacting particles, m; l is the length of the cylindrical particle, m.

The electrostatic component was calculated using eq. (6) [33, 34]:

$$U_{\text{ele,cylinder}} = \sqrt{\pi}\varepsilon\varepsilon_0\sqrt{\frac{ka_1a_2}{a_1+a_2}\cdot\left[2\sqrt{2}z_1\zeta_1z_2\zeta_2\mathrm{e}^{-kh}-(z_1^2\zeta_1^2+z_2^2\zeta_2^2)\mathrm{e}^{-2kh}\right]}, \tag{6}$$

where ζ is the electrokinetic potential, mV; z_i is the counterion charge; k is the inverse value of the thickness of the diffuse part of the electric double layer, m^{-1}; ε_0 is the dielectric constant.

3. Results and discussion

3.1. Determination of the optimal mole ratio and range of the initial concentration of the sol

According to literature [28–30] dealt with studies based on 51 V NMR method, the reaction mechanism of $V_2O_5 \cdot nH_2O$ sol can be described as follows. First, V_2O_5 dissolves in the presence of excess H_2O_2, forming an orange solution of diperoxoanions $[VO(O_2)_2]^-$. These peroxo ions are unstable in solution and gradually decompose, forming monoperoxo ions $[VO(O_2)]^+$ and then vanadate compounds. As a result, oxygen gas is released. Finally, VO_2^+ and $[H_2V_{10}O_{28}]^{4-}$ ions are obtained. Decavanadic acid $[H_2V_{10}O_{28}]^{4-}$ then spontaneously dissociates, leading to the polymerization of $V_2O_5 \cdot nH_2O$. The conversion path of peroxovanadate solutions during synthesis, according to the literatures [26] can be described as below:

$$V_2O_5{+}2H^+{+}2H_2O_2 + 3H_2O_2 \rightarrow 2VO(O)_2(OH_2)(OH_2)_3^+, \tag{7}$$

$$2V(O_2)(OH_2)_3^+{+}H_2O_2{+}H_2O_2 \rightarrow VO(O_2)_2(OH_2)^-{+}2H^+{+}2H_2O, \tag{8}$$

$$2VO(O_2)_2(OH_2)^-{+}2H^+ \rightarrow [V(O_2)_2(OH_2)]_2O^\bullet{+}H_2O, \tag{9}$$

$$[V(O_2)_2(OH_2)]2O^\bullet{+}3H_2O + 2H \rightarrow 2VO(O_2)(OH_2)_3^+{+}O_2, \tag{10}$$

$$2VO(O_2)_2(OH_2)_3^+ \rightarrow 2VO_2^+{+}O_2{+}6H_2O, \tag{11}$$

$$10VO_2^+{+}8H_2O \rightarrow H_2V_{10}O_{28}^{4-}{+}14H^+. \tag{12}$$

Therefore, based on the above literature data [26, 28–30], the reaction steps can be briefly written as shown in Fig. 1.

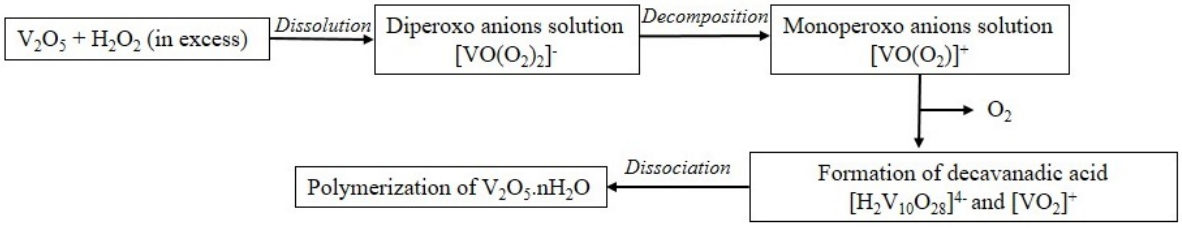

FIG. 1. Reaction steps for preparing $V_2O_5 \cdot nH_2O$ sol [26, 28–30]

To determine the optimal molar ratio for the preparation of the sol, the same mass percentage of 0.5 % was chosen under the same synthesis condition (initial mass of 0.5 g of V_2O_5 in a total sol volume of 100 ml during synthesis) according to the method of preparation shown in Section 2.2. It has been shown that at a molar ratio of $[V_2O_5]$:$[H_2O_2]$ less than [1]:[30], at the step of dissolving the V_2O_5 powder, which was the first stage of sol preparation, the powders do not completely dissolve. So for further studies, to synthesize the sols, as the minimum and optimal mole ratio for

vanadium pentoxide and hydrogen peroxide [1]:[30] was chosen. The range of sols concentrations obtained in this mole ratio that keep the sol stable for about 6 months is from 0.3 to 1.6 wt.% V_2O_5. At a content of less than 0.3 wt.% the system was in the form of a solution with precipitation, and above 1.6 % an extreme exothermic reaction occurred, and both types of sol and gel were formed. The morphology of $V_2O_5 \cdot nH_2O$ nanoparticles is shown in Fig. 2. According to Fig. 2, the solid phase is in the form of nanorods (the thickness is approximately 2 nm, the width is 15 – 25 nm, the length is 0.3 – 0.8 μm).

3.2. Determination of the actual concentration of particles and the zeta potential of the sol $\mathbf{V_2O_5 \cdot nH_2O}$

To determine the actual content of $V_2O_5 \cdot nH_2O$ nanoparticles in the sol and the loss of V_2O_5 into ionic form in aqueous medium during the synthesis of the sol $V_2O_5 \cdot nH_2O$, the ultrafiltration was carried out, and the resulting filtrate was analyzed according to the analysis procedure shown in Section 2.3. Fig. 3 shows the dependence of the percentage of $V_2O_5 \cdot nH_2O$ particles content on the amount of V_2O_5 during sol synthesis. The concentration of $V_2O_5 \cdot nH_2O$ nanoparticles increased with increasing total concentrations of vanadium (V) and it can be found that this relationship follows correctly the phase diagram of vanadium (V) in aqueous medium [35]. In addition, with increasing concentrations of vanadium (V) in the system during synthesis, the absolute value of the zeta potential of the nanoparticles increases. This occurs due to a decrease in ionic strength, since the content of dissolved vanadium ions decreases with increasing total vanadium (V) concentration of sol. The dependence of the zeta potential and ionic strength of sols on the initial concentration of V_2O_5 during synthesis are shown in Fig. 4.

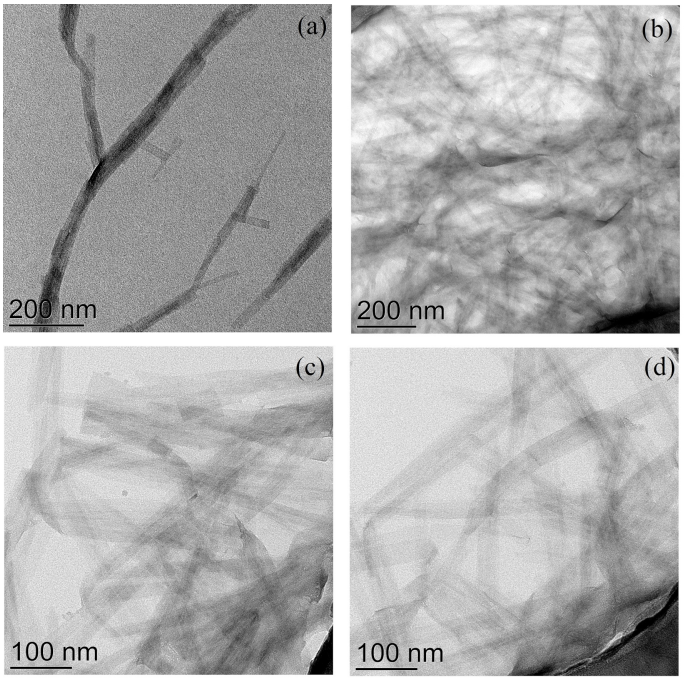

FIG. 2. TEM image of $V_2O_5 \cdot nH_2O$ nanoparticles

3.3. Determination of optical properties and the pH regions that keep the stability of sol

The optical density of the sol was analyzed using a LEKI SS2110UV spectrophotometer. To find the absorption spectrum, the sol (ω% V_2O_5 = 1) was diluted with the same pH value, and it was found that the maximum absorption spectrum was observed at 378 nm (Fig. 5). The increase in optical density with increasing concentration clearly obeys the Beer–Lambert–Bouguer law (Fig. 6).

To study the pH range that maintains the stability of the sol, it must be diluted due to the high concentration of the sol and the high optical density. The sol having a total concentration of 1 wt% V_2O_5, was diluted with the same pH number 20 times to 0.05 wt%. The initial pH of the sol is 2.45. It was found that the pH range that keeps the stability of sols is from 2.35 to 3.6, since according to the diagram of vanadium (V) in an aqueous solution [35], the solid phase of vanadium (V) exists only in a very narrow pH range in an acidic environment. As the pH decreased, the particles precipitated and then dissolved. As the pH increases, the optical density first increases, which is associated with the strengthening of the formed complex. With a further increase in pH, the optical density of the solution decreases because of the decomposition of the complex, and with a further increase in pH, partial dissolution of yellow-colored nanoparticles occurs. Optical density of the sol as a function of pH at a wavelength of 550 nm is described in Fig. 7(a).

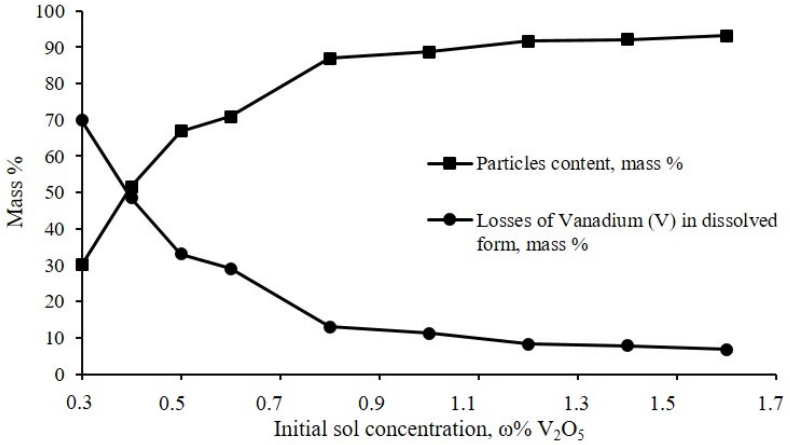

FIG. 3. Dependence of particle content and mass loss of V_2O_5 in dissolved form on the amount of V_2O_5 during sol synthesis

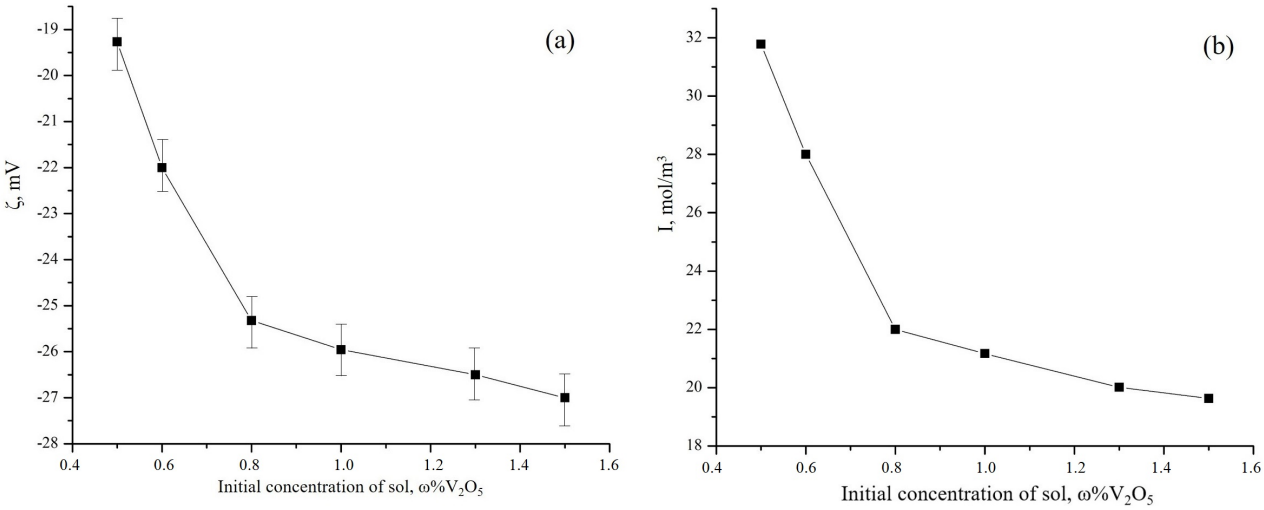

FIG. 4. Dependence of zeta potential ζ (a) and ionic strength (b) on the initial mass percentage of V_2O_5 during synthesis

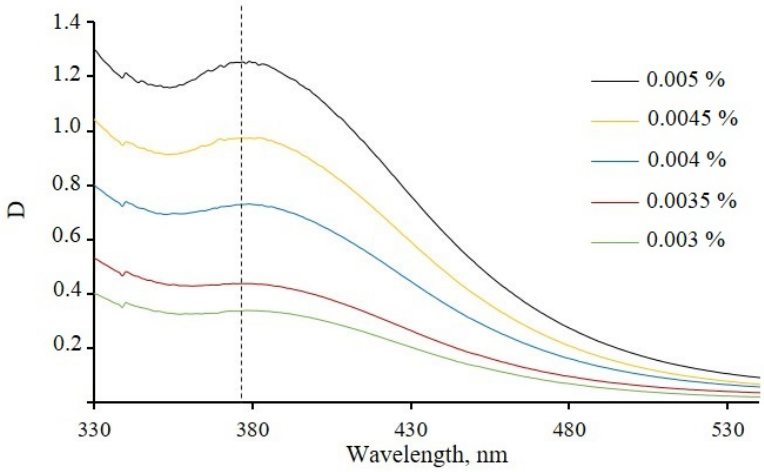

FIG. 5. Absorption spectra of sols with concentrations from 0.003 to 0.005 mass % (diluted from the initial concentration of 1 % mass)

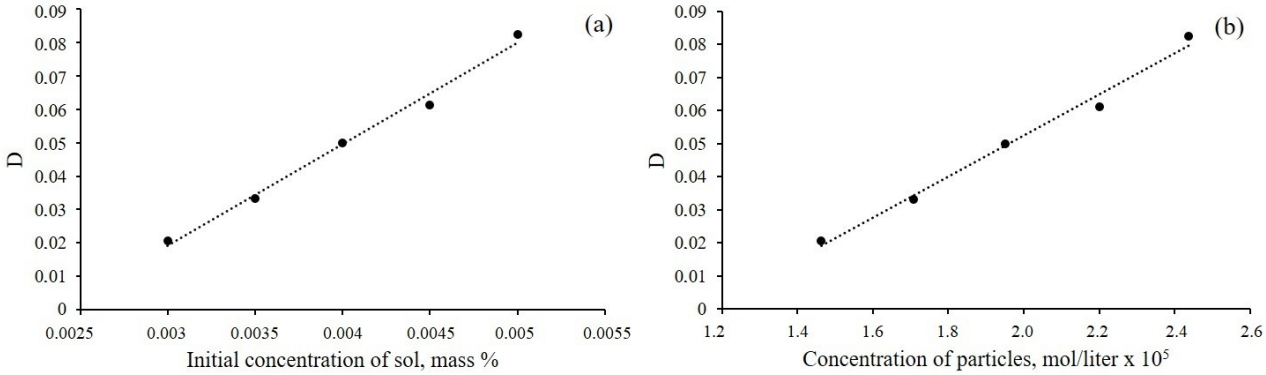

FIG. 6. Optical density of samples with different sol concentrations (a) and with different concentrations of particles at a wavelength of 378 nm (b) (diluted from the initial concentration of 1 % mass)

The dependence of the value of the zeta potential of nanoparticles on the pH of the dispersion medium was also studied, and the results are shown in Fig. 7(b). The initial value of pH is 2.45, and the concentration of sol for this experiment was taken 1 % mass V_2O_5. It was found that with increasing or decreasing the pH value from the initial pH value within the pH value that keeps sol stability, the absolute value of zeta potential is decreased. Decreasing the absolute value of zeta potential with decreasing the pH is due to the fact that point zero charge of $V_2O_5 \cdot nH_2O$ lines about at pH value 2 [36, 37]. Decreasing the absolute value of zeta potential with increasing pH is due to the dissolution of nanoparticles.

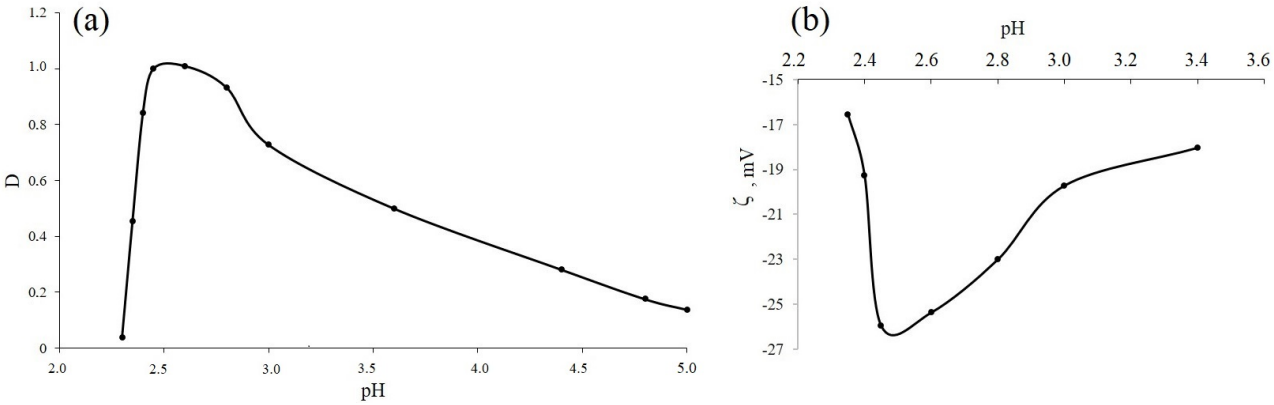

FIG. 7. Optical density of the sol (wt.% = 0.05 %, diluted from the initial concentration of 1 % wt., initial pH = 2.45) as a function of pH at a wavelength of 550 nm (a) and the dependence of the value of the zeta potential of nanoparticles on pH of the dispersion medium (concentration of sol – 1 % mass. V_2O_5, pH – 2.45) (b)

3.4. Rheological properties of the sol $V_2O_5 \cdot nH_2O$

The changes in viscosity of sol on the dependence of concentration are shown in Fig. 8(a). The viscosity of sols increases with increasing their concentration. Viscosity of sol sharply increased after the concentration of sol 1 % mass. This is due to the inner structure formation of particles. Therefore, the viscosity of sol is not linearly dependent on the concentration of sol; the system represents the lyophilic colloidal system [38]. To define the particle shape factor according to Einstein's formula [39], built the graph of the dependence of the relative viscosity of sol on the volume fraction of sol from the concentration of 0.3 to 0.9 mass % (Fig. 8(b)) as during this region the liner dependence of viscosity and concentration of sol was obtained. The particle shape factor was defined by the liner coordinate eq. (14), and its value is approximately 9.608 with a relative error value of less than 0.5 %.

$$\eta = \eta_0(1 + \alpha\varphi_{\text{effective}}), \tag{13}$$

$$\frac{\eta}{\eta_0} = 1 + \alpha\varphi_{\text{effective}}. \tag{14}$$

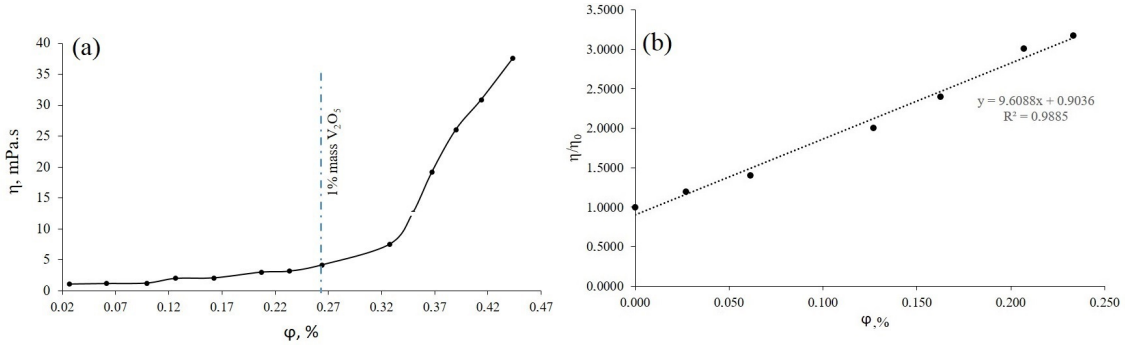

FIG. 8. The changes of viscosity of the sol on the volume fraction of the sol φ from the concentration of 0.3 to 1.6 mass % (a) and the dependence of the relative viscosity of sol η/η_0 on the volume fraction of sol φ from the concentration of 0.3 to 0.9 mass % (b)

3.5. The influence of the electrolyte on the stability of sol $V_2O_5 \cdot nH_2O$

The stability of the sol in the presence of other electrolytes in the colloidal system is one point to study the properties of sol. To determine the threshold for rapid coagulation by the optical method, the sol (ωV_2O_5 – 1 %, pH = 2.45) was diluted with the same pH value into 0.02, 0.0225, 0.025, 0.0275, 0.03, 0.04, and 0.05 mass % respectively. $NaNO_3$, singly charged counterions is used as an electrolyte. The value of the threshold for rapid coagulation is 0.03 mol/l $NaNO_3$. The dependence of the optical density of sol on the concentration of electrolyte (ωV_2O_5 – 0.03 %, pH = 2.45) is shown in Fig. 9(a). The dependence of rapid threshold coagulation on the presence of $NaNO_3$ at different pH was also studied. It was found that at the pH around 2.45 – 2.75, the rapid threshold coagulation is maximum, with incresing and decresing the pH, the value of threshold coagulation decreases as the stability of sol also decreases (Fig. 9(b)).

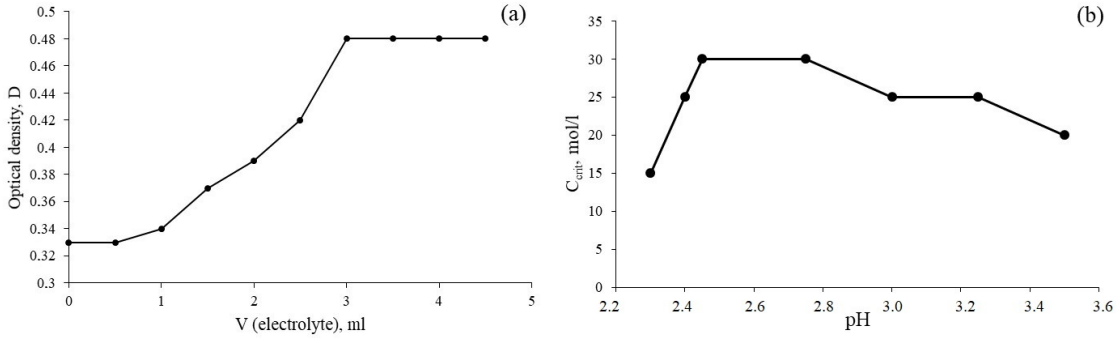

FIG. 9. The dependence of optical density of sol on the volume of electrolyte $NaNO_3$ (ωV_2O_5 – 0.03 %, pH = 2.45) (a) and the dependence of rapid threshold coagulation at the presence of $NaNO_3$ at different pH (b)

At high sol concentrations in the presence of electrolyte, the system tends to form a gel state. The dependence of the viscosity of sol (1 % mass) on the concentration of the electrolye $NaNO_3$ is shown in Fig. 10. The viscosity of lyophilic colloid sols $V_2O_5 \cdot nH_2O$ falls at small concentrations of added electrolyte $NaNO_3$ to 0.013 mol/l, and then, when the electrolyte concentration increases, it begins to increase sharply. This process can be explained by the fact that low concentrations of electrolyte destroy the internal structure of the sol due to peptization, and then at high concentrations of electrolyte, coagulation occurs and the viscosity begins to increase.

The influence of the concentration of electrolyte on the value of zeta potential of the sol was also studied (Fig. 11(a)). The zeta potential of a sol decreases when the concentration of electrolytes is increased due to the phenomenon of electrical double layer compression. When electrolytes are added to sol, they dissociate into ions, which can interact with the charged particles in the sol, neutralizing their charges. This leads to a decrease in the electrical potential at the slipping plane and thus, a decrease in the zeta potential. Additionally, the increased concentration of electrolytes can lead to the formation of a more compact and thick electrical double layer around the particles, which further reduces the magnitude of the zeta potential.

Based on the experimental results of the dependence of zeta potential on the concentration of electrolyte, the calculated value of ionic strength (I) and diffuse layer thickness (λ), and constructed natural logarithm of the zeta potential $\ln\zeta$ on the dependence of $1/\lambda$ according to liner coordinate equation Gouy–Chapman – eq. (16) [39] and the graphic is shown in Fig. 11(b).

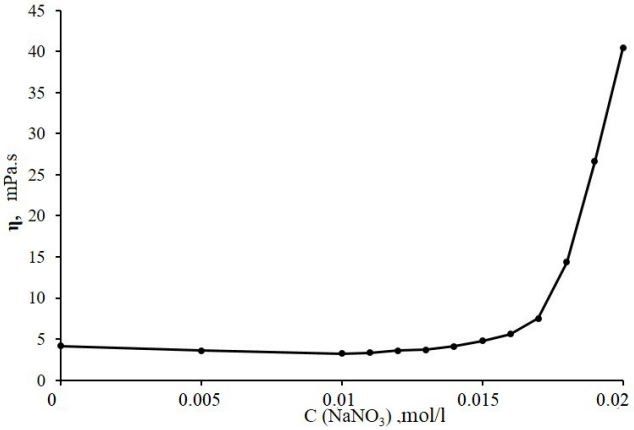

FIG. 10. The dependence of the viscosity of sol (1 % mass) on the concentration of the electrolyte $NaNO_3$

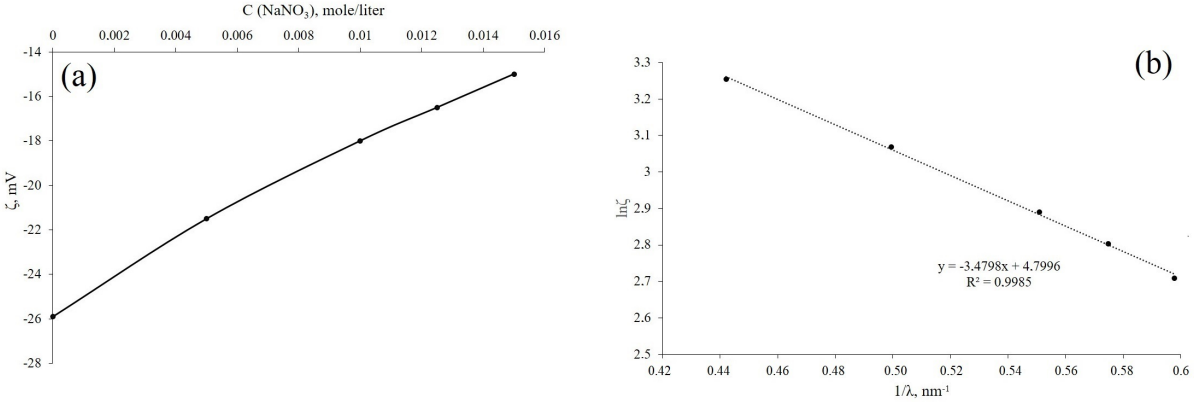

FIG. 11. The influence of the concentration of electrolyte on the value of zeta potential of the sol (concentration of sol – 1 % mass.) (a) and the dependence of natural logarithm of zeta potential $\ln\zeta$ on the value of $1/\lambda$ (b)

Gouy–Chapman equation:

$$\zeta = \varphi_\delta e^{-l/\lambda}, \tag{15}$$

$$\ln\zeta = \ln\varphi_\delta - \frac{l}{\lambda}, \tag{16}$$

where: ζ is the value of the zeta potential (mV), φ_δ is the value of the diffuse layer potential (mV), l is the distance from the Helmholtz layer to the slip plane, nm.

3.6. Calculation of potential energy of paired particle interactions using DLVO theory

Graphic of determining the value of the complex Hamaker constant for cylindrical particles of V_2O_5 sol is shown in Fig. 12(a). The graphically calculated value of the complex Hamaker constant is 2.6×10^{-20} J. As the sol $V_2O_5 \cdot nH_2O$ is very stable for about 6 months, the experimental results of potential energy of the paired particle interactions using the DLVO theory is acceptable as the energy barrier is essentially higher than the secondary mimina (Fig. 12(b)).

3.7. Determination of the dispersion phase of sol

To confirm the phase composition of dispersion phase, the sol was dried at room temperature on the glass plate. The forming thin layer was analyzed by XRD method. X-ray diffraction patterns and electron diffraction patterns of xerogel obtained after drying the sol $V_2O_5 \cdot nH_2O$ at room temperature and are shown in Fig. 13. Its X-ray diffraction peaks in Fig. 13 were in good agreement with the standard X-ray diffraction patterns of $V_2O_5 \cdot 1.6H_2O$ (JCPDS card No. 40-1296) with orthorhombic crystal system. The crystallite size in the crystallographic direction [001] was calculated using the Scherrer method and amounted to about 11 nm. The results of the interplanar distances calculated from electron diffraction data are shown in Table 1. The formation of thin layer xerogel $V_2O_5 \cdot 1.6H_2O$ on the surface of ceramic membrane is shown in Fig. 14.

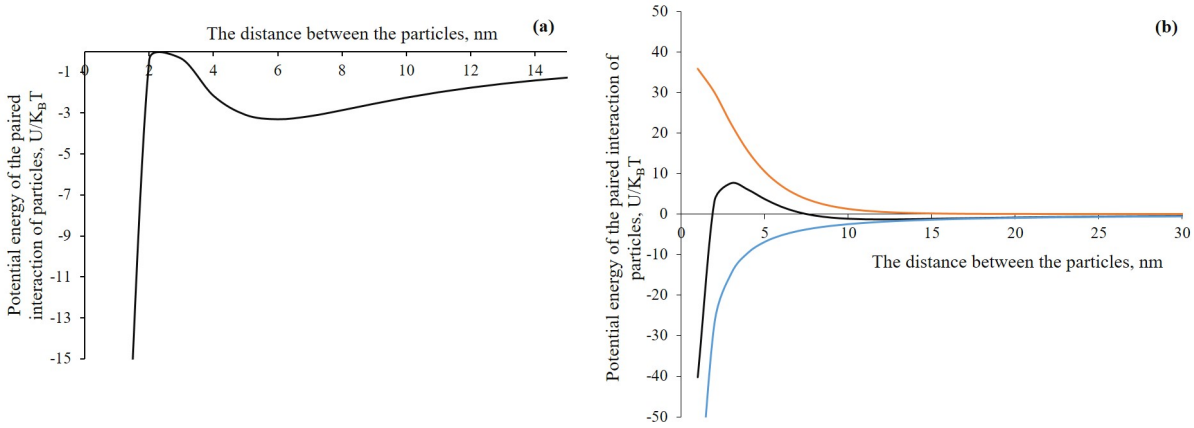

FIG. 12. Potential curves of pair interaction of $V_2O_5 \cdot nH_2O$ nanoparticles for determining the complex Hamaker constant (a) and potential curves of pair interaction of $V_2O_5 \cdot nH_2O$ nanoparticles (b)

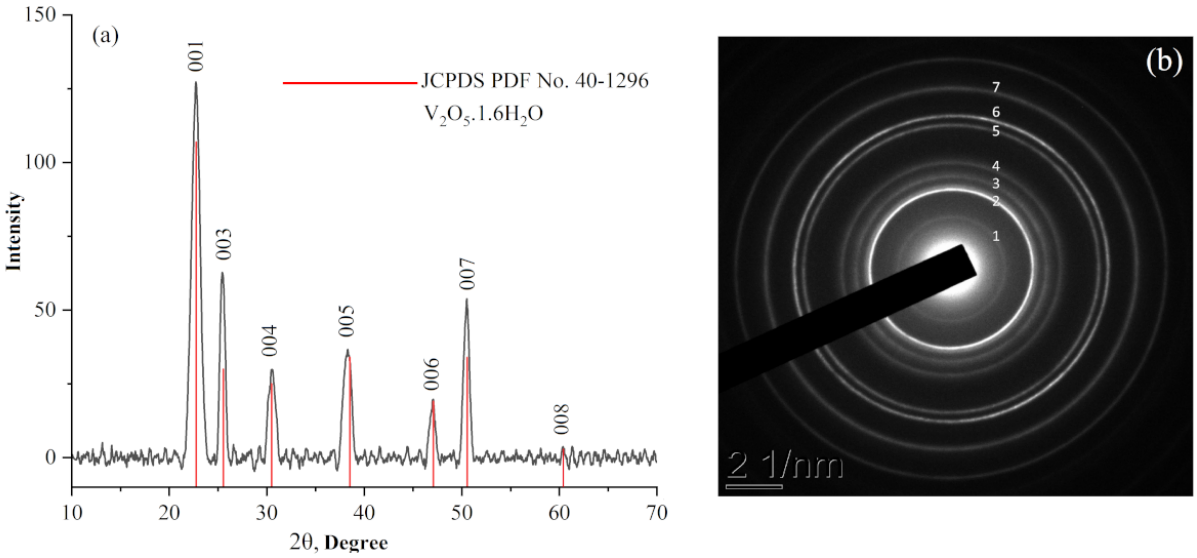

FIG. 13. X-ray diffraction patterns (a) and electron diffraction patterns (b) of xerogel obtained after drying the sol $V_2O_5 \cdot nH_2O$ at room temperature

TABLE 1. The results of comparing the interplanar distances calculated from electron diffraction data with those for the $V_2O_5 \cdot 1.6H_2O$ compound (PDF-2 No. 40-1296)

The point in Fig. 13(b)	Interplanar distances (d) according to the electron diffraction data (Fig. 13(b)), Å	Miller indices hkl of $V_2O_5 \cdot 1.6H_2O$ compound reflections
1	3.902	001
2	3.482	003
3	2.925	004
4	2.345	005
5	1.927	006
6	1.808	007
7	1.534	008

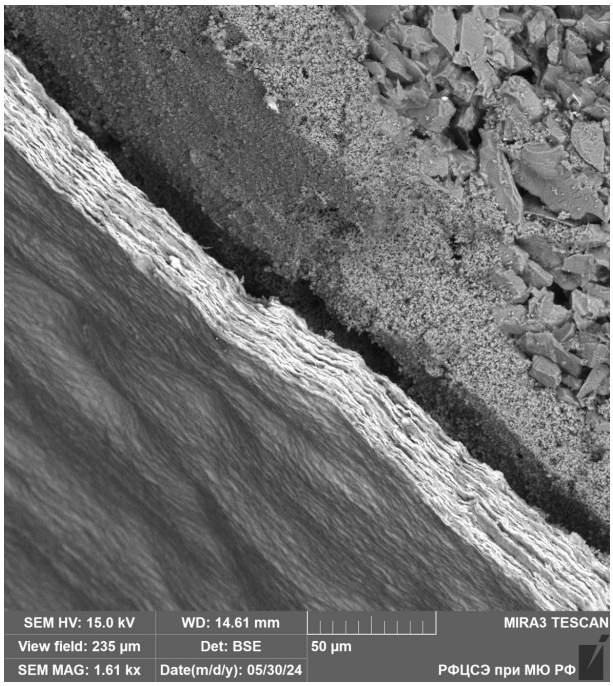

FIG. 14. SEM image of the thin film layer $V_2O_5 \cdot 1.6H_2O$, which was obtained after drying on ceramic

4. Conclusion

This study explored the colloidal chemical properties of the lyophilic dispersion system $V_2O_5 \cdot nH_2O$ sol. The key findings are as follows.

1. Optimal synthesis conditions. The optimal mole ratio of V_2O_5 and H_2O_2 for the synthesis of the sol is 1:30. The optimal concentration range that maintains the sol's stability is 0.3 to 1.6 % by mass of V_2O_5.
2. Particles content in sols. The concentration of $V_2O_5 \cdot nH_2O$ particles increased with increasing total concentrations of vanadium (V) and it can be found that this relationship follows correctly the phase diagram of vanadium (V) in aqueous medium.
3. Zeta potential. As the concentration of vanadium (V) in the system increases during synthesis, the absolute value of the zeta potential of the nanoparticles also increases as the ionic strength of the dispersion medium decreases.
4. Optical properties. The maximum absorption spectrum of the prepared sols was observed at 378 nm. The increase in optical density with increasing concentration clearly obeys the Beer-Lambert-Bouguer law.
5. pH range. The pH range that maintains the sol's stability is between 2.35 and 3.6.
6. Viscosity. The viscosity of the sol sharply increases after the concentration reaches 1 % by mass.
7. Particle shape factor. The particle shape factor is approximately 9.608, with a correlation coefficient of 0.9885.
8. The influence of the electrolyte on the stability of sol $V_2O_5 \cdot nH_2O$. The rapid threshold coagulation in the presence of $NaNO_3$ (singly charged counterions) is maximum around pH 2.45 – 2.75. At high sol concentrations in the presence of an electrolyte, the system tends to form a gel state. The zeta potential of the sol decreases when the concentration of electrolytes is increased due to the phenomenon of electrical double layer compression.
9. DLVO theory. Calculations of the potential energy of paired particle interactions using DLVO (Derjaguin–Landau–Verwey–Overbeek) theory were carried out. The experimental results of the potential energy of paired particle interactions using the DLVO theory are acceptable, as the energy barrier is significantly higher than the secondary minima.

Overall, this study provides valuable insights into the colloidal chemical properties of the $V_2O_5 \cdot nH_2O$ sol, which can be useful for various applications, such as in the development of functional materials and catalysts.

References

[1] Top K. Le, Phuong V. Pham. Recent advances in vanadium pentoxide (V_2O_5) towards related applications in chromogenics andbeyond: fundamentals, progress, and perspectives. *J. of Materials Chemistry C*, 2022, **10**, P. 1–55.

[2] Xuyan L., Jiahuan Z. V_2O_5-Based nanomaterials: synthesis and their applications. *RSC Adv.*, 2018, **8**, P. 4014–4031.

[3] Ehsan K. Recent advances in synthesis, properties, and applications of vanadium oxide nanotube. *Microchemical J.*, 2019, **145**, P. 966–978.

[4] Thi Dieu H.N., Vo K.D. Electronic and optical excitation properties of vanadium pentoxide V_2O_5. *Computational Materials Science*, 2022, **198**, P. 1–8.

[5] Sukrit S., Gaihua Ye. V_2O_5: A 2D van der Waals Oxide with Strong In-Plane Electrical and Optical Anisotropy. *ACS Appl Mater Interfaces*, 2017, **9** (28), P. 23949–23956.

[6] Ryan R.L., David M.K. Catalytic Applications of Vanadium: A Mechanistic Perspective Catalytic Applications of Vanadium: A Mechanistic Perspective. *Chemical Reviews*, 2019, **119**, P. 2128–2191.
[7] Kaichev V., Popova G.Y. Selective oxidation of methanol to form dimethoxymethane and methyl formate over a monolayer V_2O_5/TiO_2 catalyst. *J. of Catalysis*, 2014, **311**, P. 59–70.
[8] David V.F., William J.M. The formation of propane, propylene, and acetone from 2-propanol over vanadium pentoxide and modified vanadium pentoxide catalysts. *Canadian J. of Chemistry*, 1978, **56**, P. 28–39.
[9] Bars J. Le, Auroux A. Active Sites of V_2O_5/γ-Al_2O_3 catalysts in the oxidative dehydrogenation of ethane. *J. of Catalysis*, 1996, **162**, P. 250–259.
[10] Lemke K., Ehrich H. Selective hydroxylation of benzene to phenol over supported vanadium oxide catalysts. *Appl. Catal. A Gen.* 2003, **243**, P. 41–51.
[11] Lukasz W., Maria Z. Insight into pathways of methylene blue degradation with H_2O_2 over mono and bimetallic Nb, Zn oxides. *Applied Catalysis B: Environmental*, 2017, **224**, P. 634–647.
[12] Alain M., Christian M.J. V_2O_5 thin films for energy storage and conversion. *AIMS Materials Science*, 2018, **5** (3), P. 349–401.
[13] Huguenin F., Martins A.R. Nanocomposites from V_2O_5 and Lithium-Ion Batteries. In: Souza F., Leite E. (eds) *Nanoenergy*, 2017, P. 223–249.
[14] Lai V.D., To T.N. Light-assisted room temperature ammonia gas sensor based on porphyrin-coated V_2O_5 nanosheets. *Sensors and Actuators B: Chemical*, 2024, **409**, P. 135–150.
[15] Dongwon S., Jiseon K. Evaluation of V_2O_5 Film-Based Electrochromic Device with Dry-Deposited Ion Storage Layer. *Int. J. Precis. Eng. Manuf.*, 2023, **24**, P. 119–128.
[16] Ma O., Batal F.E. Impact of V_2O_5 and Gamma Ray Irradiation on the Optical and Structural FTIR Spectra of Lithium Phosphate Glass. *Global J. Eng. Sci.*, 2019, **3** (4), P. 1–8.
[17] Gary A.P., Lisa W. Effects of Aging Time on V_2O_5 Sol-Gel Coatings. *J. of Sol-Gel Science and Technology*, 1994, **3**, P. 57–62.
[18] Keiji Y., Tatsuro M. Dynamics of V_2O_5 Sol by Measurement of Ultrasonically Induced Birefringence. *J. Appl. Phys.*, 1994, **33**, P. 2901–2904.
[19] Gotic M., Popovic S. Music Sol-gel synthesis and characterization of V_2O_5 powders. *Materials Letters*, 2003, **57**, P. 3186–3192.
[20] Sanchez C., Nabavi M. Synthesis and characterization of vanadium oxide gels from alkoxy-vanadate precursors. *Mat. Res. Soc. Symp. Proc.*, 1988, **121**, P. 93–104.
[21] Wen C., Junfeng P. Synthesis of vanadium oxide nanotubes from V_2O_5 sols. *Materials Letters*, 2004, **58**, P. 2275–2278.
[22] Jay Singh, Kshitij RB Singh, Manish Kumar, Rahul Verma, Ranjana Verma, Priya Malik, Saurabh Srivastava, Ravindra Pratap Singh, Devendra Kumar. Melt-quenched vanadium pentoxide stabilized chitosan nanohybrids for efficient hydrazine detection. *Materials Advances*, 2021, **2**, P. 6665–6675.
[23] Yu H.C.W., Dai Y.M.L. Preparation and Optical Properties of V_2O_5 Nanotube Arrays. *J. of Wuhan University of Technology – Mater. Sci. Ed.*, 2006, **21**, P. 38–41.
[24] Wang N., Magdassi S., Mandler. D. Simple sol-gel process and one-step annealing of vanadium dioxide thin films: Synthesis and thermochromic properties. *Thin Solid Films*, 2013, **534**, P. 594–598.
[25] Huali W., Xuanxuan B. Open-structured $V_2O_5 \cdot nH_2O$ nanoflakes as highly reversible cathode material for monovalent and multivalent intercalation batteries. *Advanced Energy Materials*, 2017, **7**, P. 1–8.
[26] Orhan Ö., Pınar F.G. Nano-Crystal $V_2O_5 \cdot nH_2O$ Sol-Gel Films Made by Dip Coating. *AIP Proceedings*, 2012, **1476**, P. 233–240.
[27] Nathalie S., Jacques L. Rational design of one-dimensional vanadium (V) oxide nanocrystals: an insight into the physico-chemical parameters controlling the crystal structure, morphology and size of particles. *Cryst. Eng. Comm.*, 2015, **17**, P. 6780–6795.
[28] Bruno A., Jacques L. Synthesis of Vanadium Oxide Gels from Pyrovanadic Acid Solutions: A 51V NMR Study. *J. of Solid-State Chemistry*, 1999, **148**, P. 16 –19.
[29] Craig J.F., Jerzy W.W. Vanadia Gel Synthesis via Peroxovanadate Precursors. 1. In Situ Laser Raman and 51V NMR Characterization of the Gelation Process. *J. Phys. Chem. B*, 2000, **104**, P. 11622–11631.
[30] Ahmed S.E., Andrew J.P. Insights into the Exfoliation Process of $V_2O_5 \cdot nH_2O$ nanosheet Formation Using Real-Time 51V NMR. *ACS Omega*, 2019, **4**, P. 10899–10905.
[31] Muggin V.N., Khamina L.B. *Analytical chemistry of vanadium*. Publishing house "Science", Moscow, 1981, 109 p.
[32] Kirsch V.A., Kirsch V.A. Calculation of the van der Waals force between a spherical particle and an infinite cylinder. *Advances in Colloid and Interface Science*, 2003, **104**, P. 311–324.
[33] Ohshima H. *Theory of colloid and interfacial electric phenomena*. Elsevier: Ac. Press., Tokyo, 2006, 490 p.
[34] Ohshima H. *Biophysical chemistry of biointerfaces*. Wiley, Tokyo, 2010, 567 p.
[35] Povar I., Spinu O., Zinicovscaia I., Pintilie B., Ubaldini S. Revised Pourbaix diagrams for the vanadium-water system. *J. Electrochemical. Sci. Eng.*, 2019, **9**, P. 75–84.
[36] Sherif H.K., Zakya H.K. *Science and Technology of Polymers and Advanced Materials: Emerging*. Springer Science + Business Media LLC. New York, 1998, 900 p.
[37] Michael S., Karge H.G. *Advanced Zeolite Science and Applications*. Studies in Surface and Catalysts, Netherlands, 1994, 700 p.
[38] Belokon N.E. *Technical reference book for railway workers, physical and mathematical*. State Transport Railway Publishing House, Moscow, 1951, 663 p.
[39] Nazarov V.V. *Colloidal chemistry: Textbook*. Delhi Plus, Moscow, 2015, 250 p.

Submitted 22 May 2024; revised 17 August 2024; accepted 22 August 2024

Information about the authors:

Hein Myat Lwin – D. I. Mendeleev University of Chemical Technology of Russia, Department of Colloidal Chemistry, Miusskaya square, 9, Moscow, 125047, Russia; ORCID 0009-0000-6975-2380; heinmyatlwin2468@gmail.com

Oksana V. Yarovaya – D. I. Mendeleev University of Chemical Technology of Russia, Department of Colloidal Chemistry, Miusskaya square, 9, Moscow, 125047, Russia; ORCID 0000-0001-8661-3235; iarovaia.o.v@muctr.ru

Conflict of interest: the authors declare no conflict of interest.